THE JOURNAL OF PHYSICAL CHEMISTRY LETTERS
A JOURNAL OF THE AMERICAN CHEMICAL SOCIETY

pubs.acs.org/JPCL

Letter

Neural Network Quantum Molecular Dynamics, Intermediate Range Order in $GeSe_2$, and Neutron Scattering Experiments

Pankaj Rajak, Nitish Baradwaj, Ken-ichi Nomura, Aravind Krishnamoorthy, Jose P. Rino, Kohei Shimamura, Shogo Fukushima, Fuyuki Shimojo, Rajiv Kalia, Aiichiro Nakano, and Priya Vashishta*

Cite This: *J. Phys. Chem. Lett.* 2021, 12, 6020−6028

Read Online

ACCESS | Metrics & More | Article Recommendations | Supporting Information

ABSTRACT: A remarkable property of certain covalent glasses and their melts is intermediate range order, manifested as the first sharp diffraction peak (FSDP) in neutron-scattering experiments, as was exhaustively investigated by Price, Saboungi, and collaborators. Atomistic simulations thus far have relied on either quantum molecular dynamics (QMD), with systems too small to resolve FSDP, or classical molecular dynamics, without quantum-mechanical accuracy. We investigate prototypical FSDP in $GeSe_2$ glass and melt using neural-network quantum molecular dynamics (NNQMD) based on machine learning, which allows large simulation sizes with validated quantum mechanical accuracy to make quantitative comparisons with neutron data. The system-size dependence of the FSDP height is determined by comparing QMD and NNQMD simulations with experimental data. Partial pair distribution functions, bond-angle distributions, partial and neutron structure factors, and ring-size distributions are presented. Calculated FSDP heights agree quantitatively with neutron scattering data for $GeSe_2$ glass at 10 K and melt at 1100 K.

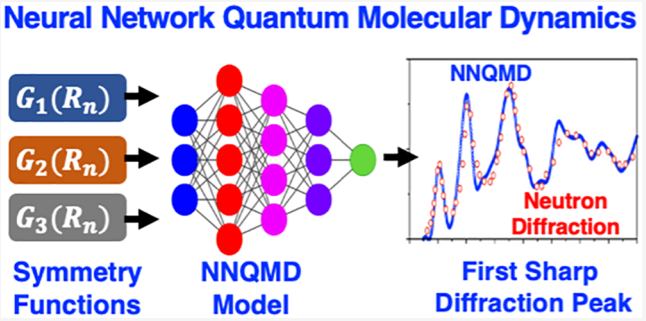

Covalent glasses such as SiO_2, $GeSe_2$, $SiSe_2$, As_2S_3, $ZnCl_2$,[1−16] and many more show intermediate range order (IRO) in real space that is manifested in wave-vector space as a first sharp diffraction peak (FSDP) in neutron and X-ray diffraction experiments.[7,17] What is remarkable is that the FSDP is also seen in the molten state of a number of chalcogenides and other covalent materials.[18] For instance, the FSDP peak found in the glassy phase of $GeSe_2$ at 10 K survives in the molten state at 1100 K with very little decrease in its intensity.[19] There has been considerable discussion about the origin of IRO and the resulting FSDP in glassy and molten states.[20,21] Beyond adjacent tetrahedra, the medium- or intermediate-range structure contains rings of tetrahedra and other inter-connected units whose exact structures are not well understood. In most neutron and X-ray experiments, only the total structure factors, $S_N(q)$ and $S_X(q)$, are determined,[22,23] and these are transformed into neutron-weighted total pair-correlation functions, $g_N(r)$; information about partial pair-correlation functions between atoms is usually not available. This information can only be obtained if tedious neutron experiments with isotope substitutions to vary neutron cross sections are carried out, which is quite rare for FSDP neutron experiments. Neutron data is often modeled using a reverse Monte Carlo method.[10,24] To explain the experimental data and to investigate the origin of the FSDP, molecular dynamics (MD) simulations using empirical inter-atomic potentials have been carried out with a considerable degree of success.[25−27] However, fully quantum mechanical calculations to achieve quantitative comparison with neutron experiments are still beyond the reach of density functional theory (DFT) computations,[28] even on petascale supercomputers, because of the $O(N^3)$ computational cost. The required size of the system to obtain pair correlations up to 30−40 Å range requires a 10 000-atom DFT-based quantum molecular dynamics (QMD) trajectory containing 50 000−100 000 MD time steps.

Great advances have been made in machine learning methods over the past few years.[29−52] In particular, deep learning methods based on neural networks have been able to learn the potential energy surface (PES) and forces from QMD trajectories of 200−400-atom systems run for 10 000−20 000 time steps, which is quite feasible with modest computing resources.[34,53−58] Using the energy and forces predicted using deep neural networks, one can accomplish two main objectives not accessible by direct DFT-based QMD simulations: (i)

Received: April 19, 2021
Accepted: May 19, 2021

https://doi.org/10.1021/acs.jpclett.1c01272
J. Phys. Chem. Lett. 2021, 12, 6020−6028

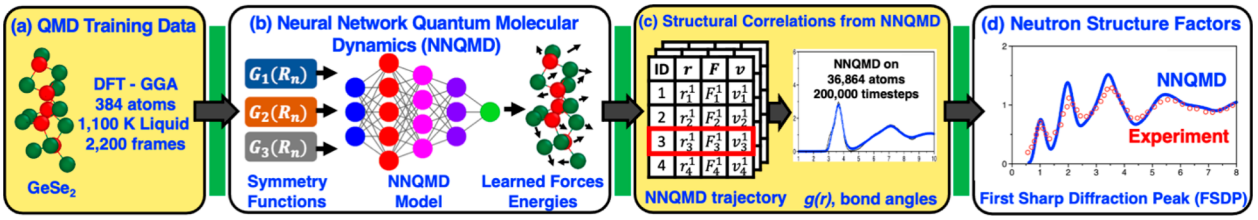

Figure 1. Proposed scheme for intermediate range order in $GeSe_2$, involving (a) QMD configurations to generate data for (b) training a neural network to learn atomic energies and forces to (c) produce NNQMD trajectories for a 36 864-atom system. (d) These atomic configurations are used to compute partial structure factors and FSDP.

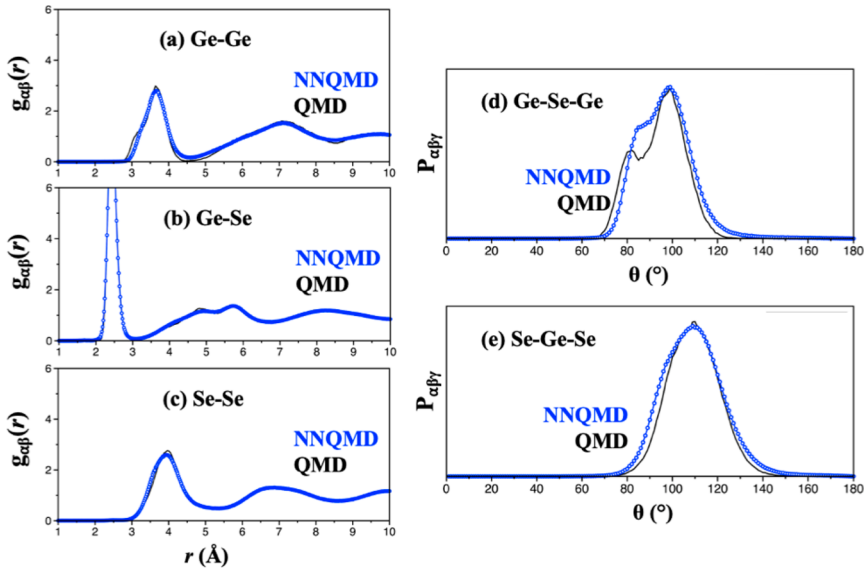

Figure 2. (a–c) Comparison of pair distribution functions, $g_{\alpha\beta}(r)$, for (a) Ge–Ge, (b) Ge–Se, and (c) Se–Se from 384-atom QMD training data (black) and 36 864-atom NNQMD (blue) of molten $GeSe_2$ at 1100 K. Comparison of bond angle distributions (d) Ge–Se–Ge and (e) Se–Ge–Se from QMD training data (black) and NNQMD (blue) at 1100 K.

compute long trajectories involving billions of time steps (microseconds) on moderate sized (10 000–100 000 atoms) systems and (ii) compute billion-atom systems where long-range defects, voids, and other phenomena between the range of 10–100 nm are important.[59]

In this paper, we report neural network quantum molecular dynamics (NNQMD) simulations with quantum mechanical accuracy for $GeSe_2$ glass at 10 K and melt at 1100 K, for a quantitative comparison of FSDP height with the neutron scattering data. Using a variety of structural correlations, we also explore the origin of IRO in real space. The approach used here provides an easily accessible method to analyze neutron scattering data for glassy and molten systems.

$GeSe_2$ is a typical chalcogenide material consisting of $Ge(Se_{1/2})_4$ tetrahedra as the building block.[60−63] In the crystalline phase $GeSe_2$ contains both edge-sharing and corner-sharing tetrahedra, which form a rather unique ring structure[64,65] of 2-, 3-, 8-, and 9-fold rings, but no 6-fold rings common to corner-sharing structures. Beside the FSDP, the ring size distributions in glassy and molten states are signatures of IRO. Because each 4-coordinated atom, Ge, participates in 6-membered rings, the ring structure and its distribution are very informative about the glassy and molten states. However, the ring structure is not an observable quantity in neutron and X-ray diffraction experiments.[66]

Figure 1 shows the proposed NNQMD-based computational scheme to characterize IRO in $GeSe_2$ and other glassy and molten materials. There are three steps in our computation of the neutron structure factor, $S_N(q)$, and the FSDP. The first step involves computation of QMD trajectories for multiple temperature–density conditions for an exhaustive sampling of the PES and forces. It is critical to perform QMD simulations that accurately reflect the PES for multiple $GeSe_2$ atomic configurations. We perform DFT simulations[67] where exchange-correlation effects are incorporated by using the Generalized Gradient Approximation (GGA) of the exchange-correlation functional,[68−70] since it was previously found that GGA is required to reproduce the FSDP in the total structure factor of molten $GeSe_2$.[71] GGA favors more ionic bonding, promoting the formation of $Ge(Se_{1/2})_4$ tetrahedra to stabilize the intermediate range ordering between intact tetrahedra that appears in the FSDP.[72] It was found that, when the Local Density Approximation is used in DFT simulations, the FSDP is not present in molten $GeSe_2$.[73] To produce training data, we use a 384-atom system of glassy and molten $GeSe_2$ using GGA-DFT in the canonical NVT ensemble for 40 000 time steps under a variety of density and temperature conditions. The second step involves training of a deep neural network (DNN) model for the PES and atomic forces on Ge and Se atoms in molten and glassy $GeSe_2$. The DNN learns a mapping from the local environment of each Ge and Se atom in the system to their atomic energy and forces, enabling large NNQMD simulations with validated accuracies of QMD at a cost comparable to that of classical MD simulations. In the third

https://doi.org/10.1021/acs.jpclett.1c01272
J. Phys. Chem. Lett. 2021, 12, 6020−6028

Table 1. Comparison of *n*-Fold Ring Statistics for Crystalline $GeSe_2$ (red), Molten 384-Atom QMD (black), and Molten 30 720-Atom NNQMD (blue) at 1100 K[a]

Ring Size	Sim.	2	3	4	5	6	7	8	9	10	11	12
Ge with **no edge** sharing tetrahedra	Crystal	0	100	0	0	0	0	100	100	0	0	0
	QMD (1100 K)	0	89	0	0	45	87	43	0	0	0	0
	NNQMD (1100 K)	0	66	8	7	7	8	53	50	3	1	1
Ge with **one edge** sharing tetrahedra	Crystal	50	50	0	0	0	0	200	0	0	0	0
	QMD (1100 K)	52	53	1	0	1	190	10	1	0	0	0
	NNQMD (1100 K)	50	49	17	13	13	17	109	17	5	2	1
Ge with **more than one** edge sharing tetrahedra	Crystal	0	0	0	0	0	0	0	0	0	0	0
	QMD (1100 K)	6	2	0	0	10	1	0	0	0	0	0
	NNQMD (1100 K)	31	18	12	8	7	6	10	5	2	1	0
Total rings per 100 Ge	Crystal	50	150	0	0	0	0	300	100	0	0	0
	QMD (1100 K)	58	144	1	1	56	279	54	1	0	0	0
	NNQMD (1100 K)	81	134	36	29	26	32	173	72	10	4	3

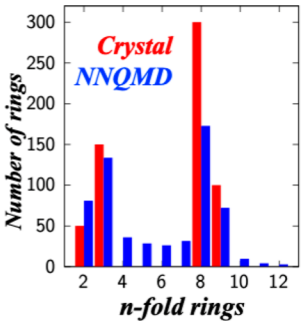

[a]The figure shows the distribution of ring sizes in crystalline and NNQMD-generated $GeSe_2$ samples. Results in the table and figure are normalized to 100 Ge for easier comparison.

step, we use NNQMD on a 36 864-atom system over 200 000 time steps (1 fs time step) to thermalize the $GeSe_2$ melt at 1100 K and create a glass by cooling the melt to 10 K at the experimental density. The accuracy of NNQMD is validated by comparing structural correlations with the QMD ground truth (Figure 2).

In this study, all QMD simulations were carried out using the VASP *ab initio* program.[74,75] The electronic states in all $GeSe_2$ systems were calculated using the projector-augmented-wave (PAW) method[76] within the framework of DFT. The exchange-correlation energy is represented by the Perdew–Burke–Ernzerhof (PBE) functional based on the GGA.[77] The plane-wave cutoff energy of 500 eV was used for the convergence of the wave function. Equations of motion for Born–Oppenheimer MD were solved via an explicit reversible integrator with a time step of 1.0 fs. The simulated $GeSe_2$ systems contained 384 atoms (128 Ge and 256 Se atoms) in an orthorhombic supercell (29.064 Å × 17.245 Å × 24.562 Å) under periodic boundary conditions. Molten systems corresponding to experimental number densities $\rho_L = 3.114 \times 10^{22}$ cm^{-3} [62] were prepared by starting from an initial configuration of the crystal.[78] The convergence criterion was set to be 10^{-5} eV for each SCF iteration.

To construct the DNN potential energy and forces for NNQMD of $GeSe_2$, the ænet package was used for the training process.[53] Training and validation data consist of 2220 QMD configurations, each with 384 (128 Ge and 256 Se) atoms. Training and validation frames are obtained by uniformly sampling every 10th frame from 22 000-step-long QMD trajectories. The atomic neighborhood was featurized according to the Behler scheme[55] using 60 radial and 36 angular symmetry functions to generate a 96-dimensional rotationally and translationally invariant feature vector. For NNQMD, we construct a DNN with two hidden layers, with 20 nodes for each layer. The "scaled hyperbolic tangent" form was used as the activation function.[53] We used the limited-memory Broyden–Fletcher–Goldfarb–Shanno method as the fitting algorithm. With these conditions, the DNN was trained to reproduce system energies and atomic forces over 500 epochs. DNN accuracy is measured against a validation set of 111 (5% of 2220 QMD configurations) frames. The root-mean-square errors for atomic energies and forces in test data after 500 epochs of training are $\Delta E = 1.59 \times 10^{-3}$ eV/atom and $\Delta F = 1.49 \times 10^{-1}$ eV/Å. More details about training methodology, feature vector construction, and metrics for NNQMD accuracy are provided in the Supporting Information. The trained DNN of the NNQMD scheme produces MD trajectories with validated quantum mechanical accuracies, given enough training data. This is shown in Figure 2a–c, where the partial pair correlation functions, $g_{\alpha\beta}(r)$, for molten $GeSe_2$ at 1100 K, computed from a 36 864-atom NNQMD simulation, are compared with the results from 384-atom QMD simulations. The NNQMD-computed $g_{\alpha\beta}(r)$ and other structure factors are fully consistent with QMD data up to 10 Å, which is larger than the range of the feature vector used in the NNQMD scheme. These plots show first-neighbor peaks in NNQMD (QMD) data corresponding to Ge–Ge, Ge–Se, and Se–Se correlations respectively at 3.66 Å (3.65 Å), 2.42 Å (2.43 Å), and 3.94 Å (3.96 Å), which are very similar to the values found in crystalline $GeSe_2$, indicating that the covalent bonding network and tetrahedral coordination around Ge in both crystalline and glassy states are similar in nature.

In addition to the pair-correlation functions, another important metric in determining the coordination of neighboring tetrahedra in these structures is the bond angles distribution between nearest-neighbor covalent bonds. Figure 2d,e shows the comparison between NNQMD and QMD bond angle distributions in molten $GeSe_2$ at 1100 K. The figures demonstrate that NNQMD has learned the PES and intra- and inter-tetrahedral co-ordinations and accurately reproduces the Se–Ge–Se bond angle of 109°, corresponding to the tetragonal angle, which compares favorably with the QMD peak position of 110°. Similarly, NNQMD produces a double-peaked distribution for Ge–Se–Ge covalent bond angles, with a shoulder at 84° and a peak at 99°, compared to QMD values of 82° and 99°. These positions correspond to central Se atoms belonging to edge-sharing and corner-sharing $Ge(Se_{1/2})_4$ tetrahedra. The broad patterns in the bond angle distributions without sharp peaks confirm that the synthesized sample is in the molten state.

While such short-range correlations of comparable quality have previously been observed in other QMD or classical MD-based simulations,[62,73,79] the true strength of the NNQMD scheme is in capturing the IRO in glassy $GeSe_2$ systems to enable a quantitative comparison with neutron experiments. Intermediate order in $GeSe_2$, which reflects the connectivity between adjacent $Ge(Se_{1/2})_4$ tetrahedra, can be inferred from statistics of *n*-fold rings structures. Table 1 shows the computed statistics of Ge–Se–Ge–Se··· *n*-fold rings in $GeSe_2$ crystal and molten $GeSe_2$. The table summarizes the total number of *n*-fold rings ($n = 2$–12) present in each of the three $GeSe_2$ systems: (a) crystalline $GeSe_2$ from experimental

https://doi.org/10.1021/acs.jpclett.1c01272
J. Phys. Chem. Lett. 2021, 12, 6020–6028

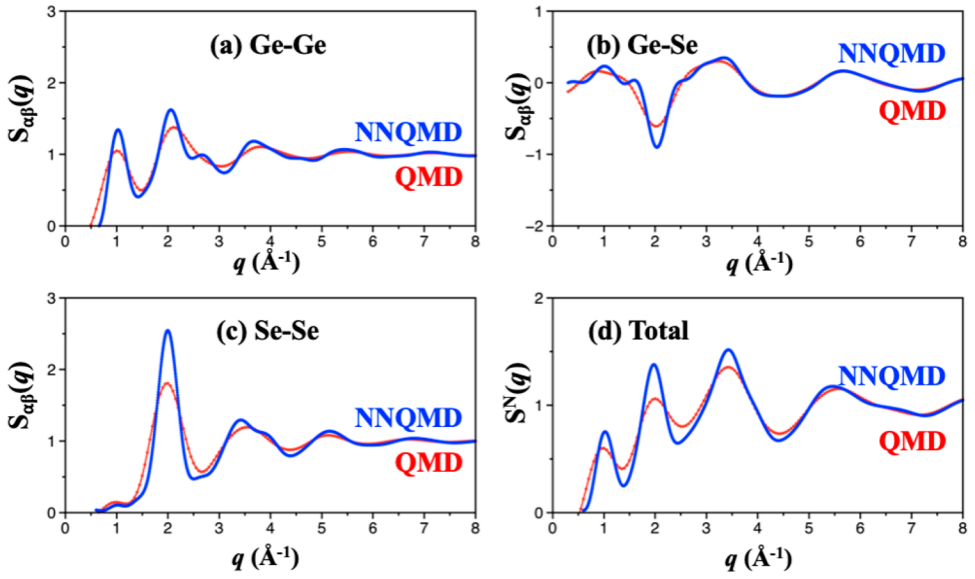

Figure 3. To show the system size effect, we compare partial structure factors $S_{\alpha\beta}(q)$ for molten $GeSe_2$ at 1100 K from 384-atom QMD (red) and 36 864-atom NNQMD (blue) (a–c), along with the total neutron structure factor $S_N(q)$ for the molten $GeSe_2$ (d).

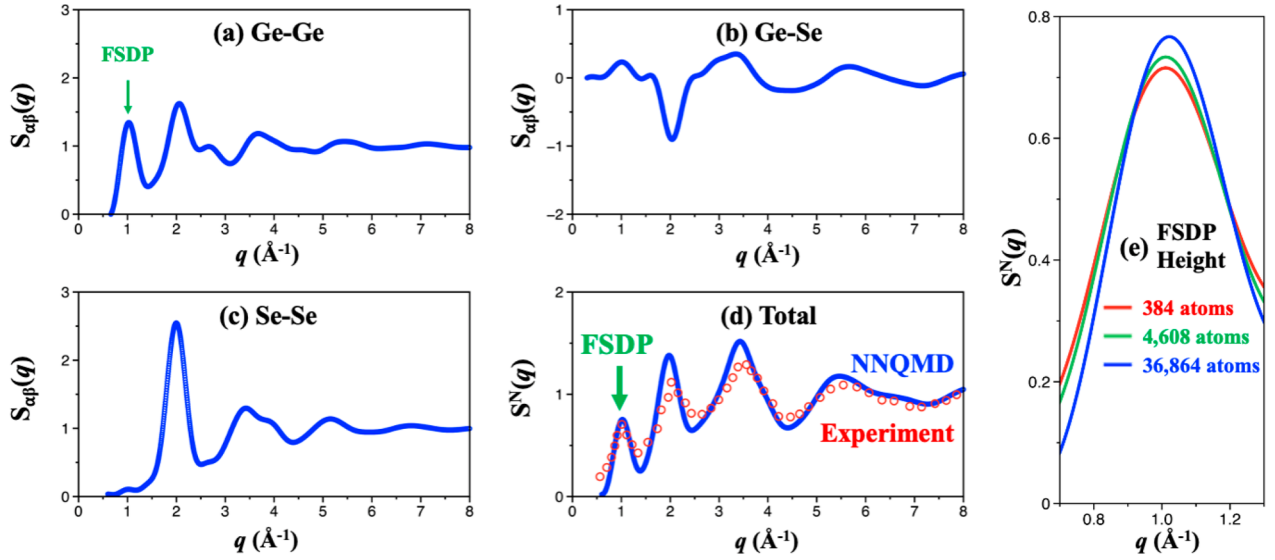

Figure 4. (a–c) Partial structure factors $S_{\alpha\beta}(q)$ for molten $GeSe_2$ from the 36 864-atom NNQMD trajectory at 1100 K. FSDP is clearly manifested in Ge–Ge correlations at 1 Å^{-1}. (d) Total neutron structure factor $S_N(q)$ for the molten $GeSe_2$ from NNQMD and experiment[9] (red circles). The FSDP is marked by a green arrow. (e) The computed height of the FSDP increases with increasing system size, saturating at a height of 0.77 for the largest system size of 36 864 atoms, consistent with experiments.

crystal structure data, (b) QMD-generated molten $GeSe_2$ at 1100 K, and (c) NNQMD-generated molten $GeSe_2$ at 1100 K. Since the ring statistics are size-extensive, the metrics computed for the three systems are normalized to 100 $GeSe_2$ molecules for easier comparison. The ring statistics for crystalline $GeSe_2$ are computed from the reported experimental crystal structure,[78] while the QMD and NNQMD statistics are computed from configurations of 384 and 30 720 atoms at 1100 K, respectively. The crystalline system contains only 2-, 3-, 8-, and 9-member rings, while the molten system in both QMD and NNQMD contains rings spanning 2–12 members. It is notable that the 8-member rings containing edge-sharing tetrahedra are substantially reduced (from 50% to 28%) on melting the crystal to produce the glassy $GeSe_2$.

The most important advantage of the NNQMD scheme lies in its ability to extend QM-accurate simulations to classical MD length and time scales, enabling computation of properties and on systems not accessible to QMD simulations. This capability allows NNQMD to bridge the gap between existing QMD calculations of the FSDP with the experimental neutron measurements. To quantify such finite-size effects in the IRO of $GeSe_2$, we compute the total structure factor, $S_N(q)$, and height of the FSDP using NNQMD for three system sizes: 384 atoms, 4608 atoms, and 36 864 atoms. All three systems are simulated at 1100 K and at identical densities of 3.98 g/cm^3. The importance of simulations on the system size is demonstrated in Figure 3a–d, which compares the $S_{\alpha\beta}(q)$ and $S_N(q)$ between a 384-atom QMD system of molten $GeSe_2$ at 1100 K and a 38 684-atom NNQMD system of molten $GeSe_2$ at the same temperature and density.

For an exhaustive comparison between neutron experiments and simulations, correlations in both r-space and q-space must

https://doi.org/10.1021/acs.jpclett.1c01272
J. Phys. Chem. Lett. 2021, 12, 6020–6028

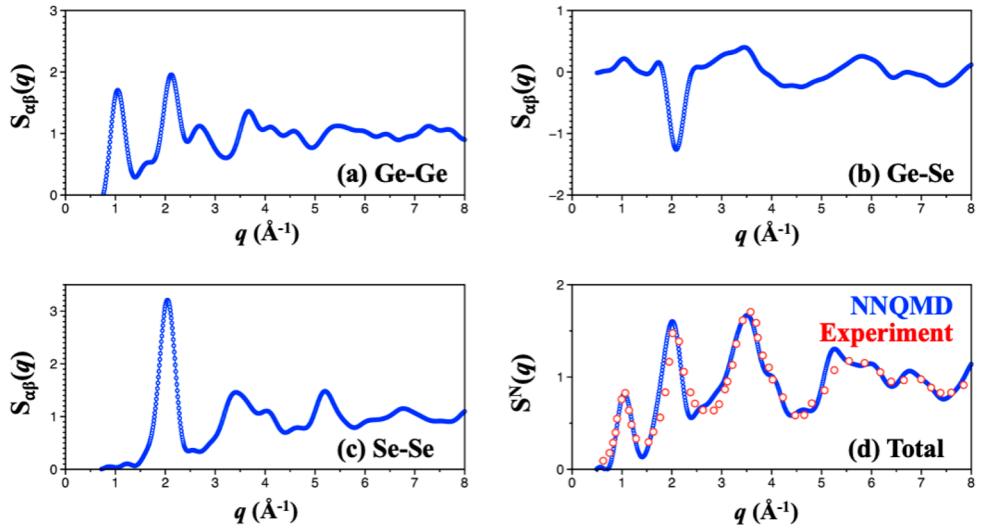

Figure 5. (a–c) NNQMD partial structure factors $S_{\alpha\beta}(q)$ for glassy $GeSe_2$ at 10 K (blue) along with (d) the 36 864-atom NNQMD neutron structure factor $S_N(q)$ for the glassy $GeSe_2$ at 10 K and the experimental neutron data for the glassy $GeSe_2$ at 10 K.[9]

be considered. In many cases, satisfactory agreement in *r*-space does not guarantee good agreement in *q*-space. For instance, Figure 2 shows acceptable agreement in *r*-space between 384-atom QMD and 36 864-atom NNQMD, but the agreement in $S_{\alpha\beta}(q)$ for the same systems shown in Figure 3 is considerably worse. The comparison with QMD simulations reveals that the smaller size of the QMD simulation cell results in lower peaks in the partial and total structure factors. The larger simulation cell possible in NNQMD increases the height and sharpness of the FSDP.[80]

Figure 4 shows the NNQMD partial structure factors $S_{\alpha\beta}(q)$ for molten $GeSe_2$ at T = 1100 K and a comparison of NNQMD $S_N(q)$ with the neutron scattering data. Our results for the $S_N(q)$ are in good agreement with the experimental data of refs 2, 8, and 19. NNQMD $S_N(q)$ shows that the FSDP has the correct height and position, in agreement with the experimental data. FSDP is the small wave vector peak (at ∼1.0 Å^{-1}), which is a universal signature of IRO.[1,81−86] From the partial structure factors, we can see that the FSDP at ∼1.0 Å^{-1} arises mainly from Ge−Ge correlations, in good agreement with prior MD data and also supported by inference from differential anomalous X-ray scattering data.[87,88] In addition to the position and height of the FSDP, the heights of other peaks in the total neutron structure factor (Figure 4d) are quantitatively consistent with prior neutron diffraction experimental data on molten $GeSe_2$.[19] This quantitative accuracy is a reflection of the extremely good representation by the NNQMD scheme to capture true quantum mechanical correlations, which are responsible for the emergence of the IRO in the molten and glassy systems. This quantitative agreement in both the position and height of the FSDP in molten $GeSe_2$ is not possible without simulations on large systems that are possible only with NNQMD. Figure 4e shows that the height of the FSDP increases in the NNQMD system with increasing system size, reaching 0.77 for the largest system size, which is in excellent agreement with neutron scattering experiments. The error of the sample mean is proportional to $1/\sqrt{N}$, where N is the number of samples. A smaller system may suffer from statistical error in the FSDP estimate, which can be substantially improved by increasing system size. Based on the sample error formula, we expect roughly an order of magnitude error reduction, $\sqrt{384/36\,864} \approx 0.1$, in the largest system size of 36 864 atoms compared to the system of 384 atoms. The second peak in the total neutron structure factor arises primarily from the Se−Se pair correlations, since the anti-correlation due to Ge−Se is overcome by Ge−Ge and Se−Se correlations.

Minor disagreements between experimental results and the results from the largest system NNQMD simulations are to be expected. QMD simulations based on DFT have inherent errors due to the use of pseudopotential approximation and local density approximation for exchange correlations. Therefore, the disagreement between experimental results and NNQMD-based simulations may be used as a guide to improve upon various approximations used in DFT-based QMD simulations. Disagreement between experimental and simulation results at 1100 K for the molten system can also be partially attributed to technical difficulties in the high-temperature neutron diffraction experiment.

The FSDP was observed in neutron and X-ray diffraction experiments on molten and glassy $GeSe_2$. NNQMD reproduces this observation as shown in Figure 5, which compares partial structure factors $S_{\alpha\beta}(q)$ and total $S_N(q)$ in the vitreous phase (T = 10 K) from NNQMD with the experimental neutron scattering data. Vitreous $GeSe_2$ structures are generated by cooling the molten $GeSe_2$ system at 1100 K in steps of 100 K down to 10 K. Subsequently, structural metrics are evaluated over 1000 MD configurations, separated by 20 time steps. It is well known from previous experiments and prior simulations that the total height of the FSDP in the glassy phases of $GeSe_2$ is slightly higher in magnitude compared to that of the molten $GeSe_2$ at 1100 K, whereas the other peaks become sharper and narrower on cooling to the glassy phase. This near-similar height of the FSDP between the molten and glassy phases is mainly a result of lower temperature for the glass density, whereas the structures of the melt and glass are topologically almost the same, as characterized by the pair-correlation functions, bond-angle distributions, and the *n*-fold ring statistics.

Having obtained quantitative agreement with neutron diffraction data for the FSDP position and height, NNQMD provides a robust method to understand the atomistic basis for

https://doi.org/10.1021/acs.jpclett.1c01272
J. Phys. Chem. Lett. 2021, 12, 6020−6028

the emergence of the IRO. The NNQMD scheme enables computation of structural metrics in real-space like $g_{\alpha\beta}(r)$ and in reciprocal space like $S_{\alpha\beta}(q)$ for a direct comparison with experiments. Both real-space and reciprocal-space comparisons are essential to obtain a comprehensive characterization of the local structure of glassy materials. The small discrepancies between NNQMD and experimental structures are inherent in the QMD simulations used for training, which are limited by approximations used in DFT (exchange-correlation and pseudopotentials). This shortcoming may be overcome by using more accurate quantum simulation techniques for generating training data, which is possible by using DFT methods that go beyond the LDA and GGA approximations to include exact exchange and higher level approximations for electronic correlations.[89−92] Alternatively, wavefunction-based methods like Green's function Monte Carlo can also be used to treat electron correlations without the constraints of an exchange-correlation approximation used in DFT, while remaining within the framework of pseudopotential approximation.[93−95] However, quantum chemistry-based higher-order methods that treat all electrons without the pseudopotential approximation, as well as techniques like CCSD(T), are currently not feasible for simulating small (384 atoms, ∼2000 valence electrons) $GeSe_2$ systems to produce training data for deep learning MD simulations.

To explain the experimental data and to investigate the origin of the FSDP in $GeSe_2$, previous MD simulations using empirical inter-atomic potentials were carried out with a considerable degree of success. These studies suggest that the FSDP in the structure factor of glassy and molten $GeSe_2$ arises from Ge−Ge correlations,[19,80,85] which can be understood as analogous to a Bragg-like peak arising from an inter-connected Ge−Ge tetrahedral network at intermediate distances. We find no evidence of layered structures at intermediate distances. Such an explanation will run counter to the observation of FSDP of nearly the same height in molten $GeSe_2$ at 1100 K. Therefore, the FSDP is better explained by a combination of steric and Coulomb forces giving rise to $Ge(Se_{1/2})_4$ tetrahedral units where the charge of a 4-fold-coordinated Ge atom is locally compensated by the 2-fold-coordinated Se atoms. These locally charge-neutral tetrahedral units form a network, and the correlations over distances characterized by the local charge-neutrality result in the FSDP.[64]

We have developed a quantum mechanically validated NNQMD scheme for the computation of structural correlations in real space and wave vector space to examine the intermediate range ordering of $GeSe_2$ in crystalline, glassy, and molten phases. This new scheme complements conventional QMD simulations and classical MD approaches based on empirical force fields by combining the quantum mechanical accuracy of QMD and the computational efficiency of MD to investigate the structural basis for the appearance of the FSDP, which is in quantitative agreement, in both position and intensity, with the experimental neutron diffraction data. Our method for analysis of IRO in molten and glassy materials is highly scalable, and its accuracy depends only on the quality of the QMD training data used to train the deep neural network. The scheme used here is quite general and may become a standard computational tool to analyze neutron scattering data for glassy and molten systems.

■ ASSOCIATED CONTENT

Supporting Information

The Supporting Information is available free of charge at https://pubs.acs.org/doi/10.1021/acs.jpclett.1c01272.

Details about NNQMD training including training accuracy, data, and symmetry functions used (PDF)

■ AUTHOR INFORMATION

Corresponding Author

Priya Vashishta − *Collaboratory for Advanced Computing and Simulations, Department of Chemical Engineering and Materials Science, Department of Physics & Astronomy, and Department of Computer Science, University of Southern California, Los Angeles 90089, United States;* orcid.org/0000-0003-4683-429X; Email: priyav@usc.edu

Authors

Pankaj Rajak − *Collaboratory for Advanced Computing and Simulations, Department of Chemical Engineering and Materials Science, Department of Physics & Astronomy, and Department of Computer Science, University of Southern California, Los Angeles 90089, United States; Argonne National Laboratory, Lemont, Illinois 60439, United States;* orcid.org/0000-0002-6344-6056

Nitish Baradwaj − *Collaboratory for Advanced Computing and Simulations, Department of Chemical Engineering and Materials Science, Department of Physics & Astronomy, and Department of Computer Science, University of Southern California, Los Angeles 90089, United States*

Ken-ichi Nomura − *Collaboratory for Advanced Computing and Simulations, Department of Chemical Engineering and Materials Science, Department of Physics & Astronomy, and Department of Computer Science, University of Southern California, Los Angeles 90089, United States*

Aravind Krishnamoorthy − *Collaboratory for Advanced Computing and Simulations, Department of Chemical Engineering and Materials Science, Department of Physics & Astronomy, and Department of Computer Science, University of Southern California, Los Angeles 90089, United States;* orcid.org/0000-0001-6778-2471

Jose P. Rino − *Departamento de Fisica, Universidade Federal de São Carlos, São Carlos, São Paulo 13565-905, Brazil*

Kohei Shimamura − *Department of Physics, Kumamoto University, Kumamoto 860-8555, Japan;* orcid.org/0000-0003-3235-2599

Shogo Fukushima − *Department of Physics, Kumamoto University, Kumamoto 860-8555, Japan*

Fuyuki Shimojo − *Department of Physics, Kumamoto University, Kumamoto 860-8555, Japan*

Rajiv Kalia − *Collaboratory for Advanced Computing and Simulations, Department of Chemical Engineering and Materials Science, Department of Physics & Astronomy, and Department of Computer Science, University of Southern California, Los Angeles 90089, United States*

Aiichiro Nakano − *Collaboratory for Advanced Computing and Simulations, Department of Chemical Engineering and Materials Science, Department of Physics & Astronomy, and Department of Computer Science, University of Southern California, Los Angeles 90089, United States;* orcid.org/0000-0003-3228-3896

Complete contact information is available at: https://pubs.acs.org/10.1021/acs.jpclett.1c01272

Notes

The authors declare no competing financial interest.

■ ACKNOWLEDGMENTS

This work was supported as part of the Computational Materials Sciences Program funded by the U.S. Department of Energy (DOE), Office of Science, Basic Energy Sciences, under Award Number DE-SC0014607. This research was partly supported by Aurora Early Science programs and used resources of the Argonne Leadership Computing Facility, which is a DOE Office of Science User Facility supported under Contract DE-AC02-06CH11357. Computations were performed at the Argonne Leadership Computing Facility under the DOE INCITE and Aurora Early Science programs and at the Center for Advanced Research Computing of the University of Southern California.

■ REFERENCES

(1) Moss, S. C.; Price, D. L., Random Packing of Structural Units and the First Sharp Diffraction Peak in Glasses. In *Physics of Disordered Materials*; Adler, D., Fritzsche, H., Ovshinsky, S. R., Eds.; Springer US: Boston, MA, 1985; pp 77−95.

(2) Price, D. L.; Moss, S. C.; Reijers, R.; Saboungi, M. L.; Susman, S. Intermediate-range order in glasses and liquids. *J. Phys.: Condens. Matter* **1989**, *1*, 1005−1008.

(3) Shpotyuk, O.; Demchenko, P.; Shpotyuk, Y.; Bujňáková, Z.; Baláž, P. Medium-range structural changes in glassy As2S3 driven by high-energy mechanical milling. *J. Non-Cryst. Solids* **2019**, *505*, 347−353.

(4) Kawasaki, M.; Kawamura, J.; Nakamura, Y.; Aniya, M. Ionic conductivity of Agx(GeSe3)1−x ($0 \leq x \leq 0.571$) glasses. *Solid State Ionics* **1999**, *123*, 259−269.

(5) Jovari, P.; Meszaros, G.; Pusztai, L.; Svab, E. Neutron diffraction studies on liquid CCl4 and C2Cl4. *Phys. B* **2000**, *276*, 491−492.

(6) Hajdu, F. Tracing the origin of the first sharp diffraction peak (FSDP) of sodium metaphosphate glass and melt. *J. Non-Cryst. Solids* **2000**, *277*, 15−21.

(7) Onodera, Y.; Kohara, S.; Salmon, P. S.; Hirata, A.; Nishiyama, N.; Kitani, S.; Zeidler, A.; Shiga, M.; Masuno, A.; Inoue, H. Structure and properties of densified silica glass: characterizing the order within disorder. *NPG Asia Mater.* **2020**, *12*, 85.

(8) Susman, S.; Price, D. L.; Volin, K. J.; Dejus, R. J.; Montague, D. G. Intermediate-range order in binary chalcogenide glasses: The first sharp diffraction peak. *J. Non-Cryst. Solids* **1988**, *106*, 26−29.

(9) Nakaoka, T.; Satoh, H.; Honjo, S.; Takeuchi, H. First-sharp diffraction peaks in amorphous GeTe and Ge2Sb2Te5 films prepared by vacuum-thermal deposition. *AIP Adv.* **2012**, *2*, 042189.

(10) Hoppe, U.; Herms, G.; Gerike, W.; Sakowski, J. The increased intensity of the first sharp diffraction peak of a NaPO3 melt. *J. Phys.: Condens. Matter* **1996**, *8*, 8077−8087.

(11) Verrall, D. J.; Gladden, L. F.; Elliott, S. R. The structure of phosphorus selenide glasses. *J. Non-Cryst. Solids* **1988**, *106*, 47−49.

(12) Horbach, J.; Kob, W.; Binder, K. Structural and dynamical properties of sodium silicate melts: an investigation by molecular dynamics computer simulation. *Chem. Geol.* **2001**, *174*, 87−101.

(13) Nakamura, M.; Arai, M.; Inamura, Y.; Otomo, T.; Bennington, S. M. Dynamical properties of vitreous silica around the first sharp diffraction peak. *Phys. Rev. B: Condens. Matter Mater. Phys.* **2003**, *67*, 064204.

(14) Du, J.; Corrales, L. R. First sharp diffraction peak in silicate glasses: Structure and scattering length dependence. *Phys. Rev. B: Condens. Matter Mater. Phys.* **2005**, *72*, 092201.

(15) Lucovsky, G.; Phillips, J. C. Nano-regime Length Scales Extracted from the First Sharp Diffraction Peak in Non-crystalline SiO2 and Related Materials: Device Applications. *Nanoscale Res. Lett.* **2010**, *5*, 550.

(16) Bychkov, E.; Benmore, C. J.; Price, D. L. Compositional changes of the first sharp diffraction peak in binary selenide glasses. *Phys. Rev. B: Condens. Matter Mater. Phys.* **2005**, *72*, 172107.

(17) Louca, D.; Poon, S. J.; Shiflet, G. J. The Effects of Sc Alloying in Y56Al24Ni10Co10 Glasses on the Local Atomic Structure. *Metall. Mater. Trans. A* **2013**, *44a*, 1990−1993.

(18) Armand, P.; Ibanez, A.; Ma, Q.; Raoux, D.; Philippot, E. Structural characterization of germanium selenide glasses by differential anomalous X-ray scattering. *J. Non-Cryst. Solids* **1994**, *167*, 37−49.

(19) Susman, S.; Volin, K. J.; Montague, D. G.; Price, D. L. The structure of vitreous and liquid GeSe2: a neutron diffraction study. *J. Non-Cryst. Solids* **1990**, *125*, 168−180.

(20) Dejus, R. J.; Susman, S.; Volin, K. J.; Montague, D. G.; Price, D. L. Structure of Vitreous Ag-Ge-Se. *J. Non-Cryst. Solids* **1992**, *143*, 162−180.

(21) Suzuya, K.; Price, D. L.; Loong, C.-K.; Martin, S. W. Intermediate- and extended-range order in phosphate glasses. *7th International Conference on the Structure of Non-Crystalline Materials*, United States, 1997-08-01.

(22) Liu, Y.; Berti, D.; Faraone, A.; Chen, W. R.; Alatas, A.; Sinn, H.; Alp, E.; Said, A.; Baglioni, P.; Chen, S. H. Inelastic X-ray scattering studies of phonons in liquid crystalline DNA. *Phys. Chem. Chem. Phys.* **2004**, *6*, 1499−1505.

(23) Sinha, S. K.; Sirota, E. B.; Garoff, S.; Stanley, H. B. X-ray and neutron scattering from rough surfaces. *Phys. Rev. B: Condens. Matter Mater. Phys.* **1988**, *38*, 2297−2311.

(24) Pusztat, L.; Mcgreevy, R. L. The Structure of Glassy Zinc-Chloride - a Reverse Monte-Carlo Study. *J. Non-Cryst. Solids* **1990**, *117*, 627−630.

(25) Skinner, L. B.; Benmore, C. J.; Weber, J. K. R.; Williamson, M. A.; Tamalonis, A.; Hebden, A.; Wiencek, T.; Alderman, O. L. G.; Guthrie, M.; Leibowitz, L.; et al. Molten uranium dioxide structure and dynamics. *Science* **2014**, *346*, 984.

(26) Krishnan, S.; Hennet, L.; Jahn, S.; Key, T. A.; Madden, P. A.; Saboungi, M.-L.; Price, D. L. Structure of Normal and Supercooled Liquid Aluminum Oxide. *Chem. Mater.* **2005**, *17*, 2662−2666.

(27) Vashishta, P.; Kalia, R. K.; Nakano, A.; Rino, J. P. Interaction potentials for alumina and molecular dynamics simulations of amorphous and liquid alumina. *J. Appl. Phys.* **2008**, *103*, 083504.

(28) Hohenberg, P.; Kohn, W. The Inhomogeneous Electron Gas. *Phys. Rev.* **1964**, *136*, B864−B864.

(29) Mocanu, F. C.; Konstantinou, K.; Lee, T. H.; Bernstein, N.; Deringer, V. L.; Csanyi, G.; Elliott, S. R. Modeling the Phase-Change Memory Material, $Ge_2Sb_2Te_5$, with a Machine-Learned Interatomic Potential. *J. Phys. Chem. B* **2018**, *122*, 8998−9006.

(30) Bartok, A. P.; Payne, M. C.; Kondor, R.; Csanyi, G. Gaussian Approximation Potentials: The Accuracy of Quantum Mechanics, without the Electrons. *Phys. Rev. Lett.* **2010**, *104*, 136403.

(31) Bernstein, N.; Csányi, G.; Deringer, V. L. De novo exploration and self-guided learning of potential-energy surfaces. *Npj Comput. Mater.* **2019**, *5*, 99.

(32) Cubuk, E. D.; Schoenholz, S. S.; Kaxiras, E.; Liu, A. J. Structural Properties of Defects in Glassy Liquids. *J. Phys. Chem. B* **2016**, *120*, 6139−6146.

(33) Cubuk, E. D.; Schoenholz, S. S.; Rieser, J. M.; Malone, B. D.; Rottler, J.; Durian, D. J.; Kaxiras, E.; Liu, A. J. Identifying Structural Flow Defects in Disordered Solids Using Machine-Learning Methods. *Phys. Rev. Lett.* **2015**, *114*, 108001.

(34) Fukushima, S.; Ushijima, E.; Kumazoe, H.; Koura, A.; Shimojo, F.; Shimamura, K.; Misawa, M.; Kalia, R. K.; Nakano, A.; Vashishta, P. Thermodynamic integration by neural network potentials based on first-principles dynamic calculations. *Phys. Rev. B: Condens. Matter Mater. Phys.* **2019**, *100*, 214108.

(35) Shimamura, K.; Fukushima, S.; Koura, A.; Shimojo, F.; Misawa, M.; Kalia, R. K.; Nakano, A.; Vashishta, P.; Matsubara, T.; Tanaka, S. Guidelines for creating artificial neural network empirical interatomic potential from first-principles molecular dynamics data under specific

https://doi.org/10.1021/acs.jpclett.1c01272
J. Phys. Chem. Lett. 2021, 12, 6020−6028

conditions and its application to alpha-Ag_2Se. *J. Chem. Phys.* **2019**, *151*, 124303.
(36) Pyzer-Knapp, E. O.; Li, K. W.; Aspuru-Guzik, A. Learning from the Harvard Clean Energy Project: The Use of Neural Networks to Accelerate Materials Discovery. *Adv. Funct. Mater.* **2015**, *25*, 6495−6502.
(37) Li, Z. W.; Kermode, J. R.; De Vita, A. Molecular Dynamics with On-the-Fly Machine Learning of Quantum-Mechanical Forces. *Phys. Rev. Lett.* **2015**, *114*, 096405.
(38) Behler, J. Perspective: Machine learning potentials for atomistic simulations. *J. Chem. Phys.* **2016**, *145*, 170901.
(39) Carrasquilla, J.; Melko, R. G. Machine learning phases of matter. *Nat. Phys.* **2017**, *13*, 431−434.
(40) Sanchez-Lengeling, B.; Aspuru-Guzik, A. Inverse molecular design using machine learning: Generative models for matter engineering. *Science* **2018**, *361*, 360−365.
(41) Butler, K. T.; Davies, D. W.; Cartwright, H.; Isayev, O.; Walsh, A. Machine learning for molecular and materials science. *Nature* **2018**, *559*, 547−555.
(42) Artrith, N.; Urban, A.; Ceder, G. Efficient and accurate machine-learning interpolation of atomic energies in compositions with many species. *Phys. Rev. B: Condens. Matter Mater. Phys.* **2017**, *96*, 014112.
(43) Cubuk, E. D.; Ivancic, R. J. S.; Schoenholz, S. S.; Strickland, D. J.; Basu, A.; Davidson, Z. S.; Fontaine, J.; Hor, J. L.; Huang, Y. R.; Jiang, Y.; et al. Structure-property relationships from universal signatures of plasticity in disordered solids. *Science* **2017**, *358*, 1033−1037.
(44) Ren, F.; Ward, L.; Williams, T.; Laws, K. J.; Wolverton, C.; Hattrick-Simpers, J.; Mehta, A. Accelerated discovery of metallic glasses through iteration of machine learning and high-throughput experiments. *Science Advances* **2018**, *4*, eaaq1566.
(45) Ye, W. K.; Chen, C.; Wang, Z. B.; Chu, I. H.; Ong, S. P. Deep neural networks for accurate predictions of crystal stability. *Nat. Commun.* **2018**, *9*, 3800.
(46) Huan, T. D.; Batra, R.; Chapman, J.; Krishnan, S.; Chen, L.; Ramprasad, R. A universal strategy for the creation of machine learning-based atomistic force fields. *Npj Comput. Mater.* **2017**, *3*, 37.
(47) Chmiela, S.; Sauceda, H. E.; Muller, K. R.; Tkatchenko, A. Towards exact molecular dynamics simulations with machine-learned force fields. *Nat. Commun.* **2018**, *9*, 3887.
(48) Sosso, G. C.; Miceli, G.; Caravati, S.; Behler, J.; Bernasconi, M. Neural network interatomic potential for the phase change material GeTe. *Phys. Rev. B: Condens. Matter Mater. Phys.* **2012**, *85*, 174103.
(49) Smith, J. S.; Isayev, O.; Roitberg, A. E. ANI-1: an extensible neural network potential with DFT accuracy at force field computational cost. *Chem. Sci.* **2017**, *8*, 3192−3203.
(50) Zhang, L. F.; Chen, M. H.; Wu, X. F.; Wang, H.; Weinan, E.; Car, R. Deep neural network for the dielectric response of insulators. *Phys. Rev. B: Condens. Matter Mater. Phys.* **2020**, *102*, 041121.
(51) Yao, K.; Herr, J. E.; Toth, D. W.; Mckintyre, R.; Parkhill, J. The TensorMol-0.1 model chemistry: a neural network augmented with long-range physics. *Chem. Sci.* **2018**, *9*, 2261−2269.
(52) Schutt, K. T.; Kindermans, P. J.; Sauceda, H. E.; Chmiela, S.; Tkatchenko, A.; Muller, K. R. SchNet: A Continuous-Filter Convolutional Neural Network for Modeling Quantum Interactions. *Nips'17* **2017**, 992−1002.
(53) Artrith, N.; Urban, A. An implementation of artificial neural-network potentials for atomistic materials simulations: Performance for TiO_2. *Comput. Mater. Sci.* **2016**, *114*, 135−150.
(54) Behler, J. First Principles Neural Network Potentials for Reactive Simulations of Large Molecular and Condensed Systems. *Angew. Chem., Int. Ed.* **2017**, *56*, 12828−12840.
(55) Behler, J.; Parrinello, M. Generalized neural-network representation of high-dimensional potential-energy surfaces. *Phys. Rev. Lett.* **2007**, *98*, 146401.
(56) Botu, V.; Batra, R.; Chapman, J.; Ramprasad, R. Machine Learning Force Fields: Construction, Validation, and Outlook. *J. Phys. Chem. C* **2017**, *121*, 511−522.
(57) Deringer, V. L.; Caro, M. A.; Csanyi, G. Machine Learning Interatomic Potentials as Emerging Tools for Materials Science. *Adv. Mater.* **2019**, *31*, 1902765.
(58) Unke, O. T.; Meuwly, M. PhysNet: A Neural Network for Predicting Energies, Forces, Dipole Moments, and Partial Charges. *J. Chem. Theory Comput.* **2019**, *15*, 3678−3693.
(59) Rajak, P.; Liu, K.; Krishnamoorthy, A.; Kalia, R. K.; Nakano, A.; Nomura, K. i.; Tiwari, S. C.; Vashishta, P. Neural Network Molecular Dynamics at Scale *2020 IEEE International Parallel and Distributed Processing Symposium Workshops (IPDPSW)*, May 2020; 2020; pp 991−994.
(60) Salmon, P. S. Structure of liquids and glasses in the Ge−Se binary system. *J. Non-Cryst. Solids* **2007**, *353*, 2959−2974.
(61) Penfold, I. T.; Salmon, P. S. A neutron diffraction study on the structure of molten GeSe2: the Ge coordination environment. *J. Phys.: Condens. Matter* **1990**, *2*, SA233−SA237.
(62) Vashishta, P.; Kalia, R. K.; Antonio, G. A.; Ebbsjö, I. Atomic correlations and intermediate-range order in molten and amorphous ${\mathrm{GeSe}}_{2}$. *Phys. Rev. Lett.* **1989**, *62*, 1651−1654.
(63) Antonio, G. A.; Kalia, R. K.; Vashishta, P. Sise2 Glass - a Molecular-Dynamics Study. *J. Non-Cryst. Solids* **1988**, *106*, 305−308.
(64) Iyetomi, H.; Vashishta, P.; Kalia, R. K. Integral-equation theory of the origin of medium-range order in molten and vitreous chalcogenides. *J. Phys.: Condens. Matter* **1989**, *1*, 2103−2107.
(65) Iyetomi, H.; Vashishta, P.; Kalia, R. K. Integral-equation approach to medium-range order in molten and glassy chalcogenides. *Phys. Rev. B: Condens. Matter Mater. Phys.* **1991**, *43*, 1726−1734.
(66) Rino, J. P.; Ebbsjo, I.; Kalia, R. K.; Nakano, A.; Vashishta, P. Structure of Rings in Vitreous SiO2. *Phys. Rev. B: Condens. Matter Mater. Phys.* **1993**, *47*, 3053−3062.
(67) Kohn, W.; Vashishta, P., General Density Functional Theory. In *Theory of the Inhomogeneous Electron Gas*, Lundqvist, S.; March, N. H., Eds. Springer US: Boston, MA, 1983; pp 79−147.
(68) Ji, M.; Umemoto, K.; Wang, C. Z.; Ho, K. M.; Wentzcovitch, R. M. Ultrahigh-pressure phases of H2O ice predicted using an adaptive genetic algorithm. *Phys. Rev. B: Condens. Matter Mater. Phys.* **2011**, *84*, 220105.
(69) Zhao, X. F.; Yang, X. Y.; Li, Y. X.; Ahuja, R. Exploring the Degradation Behavior of Ce-Monazite in Water Solution through Adsorption and Penetration Kinetics. *J. Phys. Chem. C* **2020**, *124*, 22173−22184.
(70) Le, D.; Rawal, T. B.; Rahman, T. S. Single-Layer MoS2 with Sulfur Vacancies: Structure and Catalytic Application. *J. Phys. Chem. C* **2014**, *118*, 5346−5351.
(71) Massobrio, C.; Pasquarello, A.; Car, R. Microscopic Structure of Liquid ${\mathrm{GeSe}}{}_{2}$: The Problem of Concentration Fluctuations over Intermediate Range Distances. *Phys. Rev. Lett.* **1998**, *80*, 2342−2345.
(72) Massobrio, C.; Pasquarello, A. Origin of the first sharp diffraction peak in the structure factor of disordered network-forming systems: Layers or voids? *J. Chem. Phys.* **2001**, *114*, 7976−7979.
(73) Massobrio, C.; Pasquarello, A.; Car, R. Intermediate Range Order and Bonding Character in Disordered Network-Forming Systems. *J. Am. Chem. Soc.* **1999**, *121*, 2943−2944.
(74) Kresse, G.; Furthmuller, J. Efficient iterative schemes for ab initio total-energy calculations using a plane-wave basis set. *Phys. Rev. B: Condens. Matter Mater. Phys.* **1996**, *54*, 11169−11186.
(75) Kresse, G.; Furthmuller, J. Efficiency of ab-initio total energy calculations for metals and semiconductors using a plane-wave basis set. *Comput. Mater. Sci.* **1996**, *6*, 15−50.
(76) Kresse, G.; Joubert, D. From ultrasoft pseudopotentials to the projector augmented-wave method. *Phys. Rev. B: Condens. Matter Mater. Phys.* **1999**, *59*, 1758−1775.
(77) Perdew, J. P.; Burke, K.; Ernzerhof, M. Generalized Gradient Approximation Made Simple. *Phys. Rev. Lett.* **1996**, *77*, 3865−3868.
(78) Dittmar, G.; Schafer, H. Die Kristallstruktur von Germaniumdiselenid. *Acta Crystallogr., Sect. B: Struct. Crystallogr. Cryst. Chem.* **1976**, *32*, 2726−2728.

https://doi.org/10.1021/acs.jpclett.1c01272
J. Phys. Chem. Lett. 2021, 12, 6020−6028

(79) Massobrio, C.; Pasquarello, A.; Car, R. Short- and intermediate-range structure of liquid ${\mathrm{GeSe}}_{2}$. *Phys. Rev. B: Condens. Matter Mater. Phys.* **2001**, *64*, 144205.
(80) Tanaka, K. Medium-Range Structure in Chalcogenide Glasses. *Jpn. J. Appl. Phys.* **1998**, *37*, 1747−1753.
(81) Elliott, S. R. The origin of the first sharp diffraction peak in the structure factor of covalent glasses and liquids. *J. Phys.: Condens. Matter* **1992**, *4*, 7661−7678.
(82) Elliott, S. R. Extended-Range Order, Interstitial Voids and the First Sharp Diffraction Peak of Network Glasses. *J. Non-Cryst. Solids* **1995**, *182*, 40−48.
(83) Fischer, H. E.; Barnes, A. C.; Salmon, P. S. Neutron and x-ray diffraction studies of liquids and glasses. *Rep. Prog. Phys.* **2006**, *69*, 233−299.
(84) Micoulaut, M.; Bauchy, M. Anomalies of the first sharp diffraction peak in network glasses: Evidence for correlations with dynamic and rigidity properties. *Phys. Status Solidi B* **2013**, *250*, 976−982.
(85) Penfold, I. T.; Salmon, P. S. Structure of covalently bonded glass-forming melts: A full partial-structure-factor analysis of liquid ${\mathrm{GeSe}}_{2}$. *Phys. Rev. Lett.* **1991**, *67*, 97−100.
(86) Salmon, P. S. Real space manifestation of the first sharp diffraction peak in the structure factor of liquid and glassy materials. *Proc. R. Soc. London. Series A: Mathematical and Physical Sciences* **1994**, *445*, 351−365.
(87) Fuoss, P. H.; Eisenberger, P.; Warburton, W. K.; Bienenstock, A. Application of Differential Anomalous X-Ray Scattering to Structural Studies of Amorphous Materials. *Phys. Rev. Lett.* **1981**, *46*, 1537−1540.
(88) Fuoss, P. H.; Fischer-Colbrie, A. Structure of a-${\mathrm{GeSe}}_{2}$ from x-ray scattering measurements. *Phys. Rev. B: Condens. Matter Mater. Phys.* **1988**, *38*, 1875−1878.
(89) Shao, M.; Lin, L.; Yang, C.; Liu, F.; Da Jornada, F. H.; Deslippe, J.; Louie, S. G. Low rank approximation in G0W0 calculations. *Science China Mathematics* **2016**, *59*, 1593−1612.
(90) Louie, S. G.; Rubio, A., Quasiparticle and Optical Properties of Solids and Nanostructures: The GW-BSE Approach. In *Handbook of Materials Modeling: Methods*, Yip, S., Ed. Springer Netherlands: Dordrecht, 2005; pp 215−240.
(91) Govoni, M.; Galli, G. Large Scale GW Calculations. *J. Chem. Theory Comput.* **2015**, *11*, 2680−2696.
(92) Jain, A.; Shin, Y.; Persson, K. A. Computational predictions of energy materials using density functional theory. *Nat. Rev. Mater.* **2016**, *1*, 15004.
(93) Tubman, N. M.; Kylänpää, I.; Hammes-Schiffer, S.; Ceperley, D. M. Beyond the Born-Oppenheimer approximation with quantum Monte Carlo methods. *Phys. Rev. A: At., Mol., Opt. Phys.* **2014**, *90*, 042507.
(94) Shin, H.; Krogel, J. T.; Gasperich, K.; Kent, P. R. C.; Benali, A.; Heinonen, O. Optimized structure and electronic band gap of monolayer GeSe from quantum Monte Carlo methods. *Phy Rev. Mater.* **2021**, *5*, 024002.
(95) Kent, P. R. C.; Kotliar, G. Toward a predictive theory of correlated materials. *Science* **2018**, *361*, 348.

https://doi.org/10.1021/acs.jpclett.1c01272
J. Phys. Chem. Lett. 2021, 12, 6020−6028